

Analytical Emulator for the Linear Matter Power Spectrum from Physics-Informed Machine Learning

J. Bayron Orjuela-Quintana,^{1, 2, *} Domenico Sapone,^{2, †} and Savvas Nesseris^{3, ‡}

¹Departamento de Física, Universidad del Valle,

Ciudad Universitaria Meléndez, Santiago de Cali 760032, Colombia

²Cosmology and Theoretical Astrophysics group, Departamento de Física,

FCFM, Universidad de Chile, Blanco Encalada 2008, Santiago, Chile

³Instituto de Física Teórica UAM-CSIC, Universidad Autonóma de Madrid, Cantoblanco, 28049 Madrid, Spain

Current and future large-scale structure surveys aim to constrain cosmological parameters with unprecedented precision by analyzing vast amounts of data. This imposes a pressing need to develop fast and accurate methods for computing the matter power spectrum $P(k)$, or equivalently, the matter transfer function $T(k)$. In previous works, we introduced precise fitting formulas for these quantities within the standard cosmological model, including extensions such as the presence of massive neutrinos and modifications of gravity. However, these formulations overlooked a key characteristic imprinted in $P(k)$: the baryon acoustic oscillation signal. Here, we leverage our understanding of the well-known physics behind this oscillatory pattern to impose constraints on our genetic algorithm, a machine learning technique. By employing this “physics-informed” approach, we introduce an expression that accurately describes the matter transfer function with sub-percent mean accuracy. The high interpretability of the output allows for straightforward extensions of this formulation to other scenarios involving massive neutrinos and modifications of gravity. We anticipate that this formula will serve as a competitive fitting function for $P(k)$, meeting the accuracy requirements essential for cosmological analyses.

I. INTRODUCTION

Symbolic Regression (SR), i.e., the task of finding a mathematical expression that accurately captures the relationship between variables and parameters from observational data, has been fundamental to the advancement of physics. Traditionally, this task was performed manually by scientists; however, modern computational algorithms now facilitate this process by systematically exploring the “model” space to fit given datasets corresponding to physical phenomena.

When the target model is expressed using simple functions—such as trigonometric, exponential, and polynomial functions—randomly combined to fit the data, the number of possible combinations grows exponentially. This combinatorial explosion can be managed using machine learning techniques that efficiently identify incorrect and correct paths to accurately describe the data. These algorithms seek to compress and manipulate datasets to uncover patterns in them. These patterns will correspond to “laws of physics” or, at least, to approximations thereof [1–4].

Among these machine learning-based algorithms is the publicly available **AI-Feynman** code [5–7]. **AI-Feynman** is a neural network-based tool trained to

recognize properties essential in physics, such as symmetries, separability, compositionality, and simplification. By incorporating these “physics-inspired” heuristics, **AI-Feynman** has successfully rediscovered 100 physical relationships detailed in the famous Feynman Lectures on Physics, albeit in somewhat idealised conditions.

Genetic programming (GP), which is another machine learning method, offers a different strategy to navigate the vast model space inherent in brute-force symbolic regression methods. Similar to the Markov chain Monte Carlo (MCMC) method used in parameter space exploration, a Genetic Algorithm (GA) traverse the model space by accepting or rejecting candidate expressions based on their fitness, which measures how well they fit the given data. This evolutionary approach enables GAs to efficiently explore the model space, avoiding the combinatorial explosion of possible solutions and converging on accurate and interpretable expressions [8].

In cosmology, the matter power spectrum, $P(k)$, is a critical quantity linking observations with theoretical predictions [9–11]. Recent large-scale structure surveys, such as Euclid [12, 13] and DESI [14], aim to constrain cosmological parameters with unprecedented precision by comparing their observations with the predictions of relevant summary statistics, such as the matter power spectrum. Consequently, there is a pressing need for fast and accurate computations of $P(k)$ [15]. In previous works, we have employed GAs to derive simple and precise expressions for the linear matter power spectrum

* john.orjuela@correounivalle.edu.co

† domenico.sapone@uchile.cl

‡ savvas.nesseris@csic.es

within the standard cosmological model [16], incorporating the effects of one massive neutrino and various modifications of gravity [17]. However, these formulations neglected one of $P(k)$'s most distinctive features: the oscillatory pattern at intermediate scales, known as the Baryon Acoustic Oscillations (BAO) signal [18]. In this work, we extend our previous efforts by using GAs to model this oscillatory pattern.

The physics underlying the wiggles in $P(k)$ is well understood, originating from pressure-induced oscillations in the early universe when baryons were tightly coupled to photons via Compton scattering [11]. We propose a methodology where the model space is highly constrained by this physical knowledge, akin to setting priors in an MCMC run. Our algorithm targets predefined functions to describe the matter power spectrum's oscillations below the sound horizon, with an asymptotic amplitude determined by the matter content of the universe and an exponential suppression at small scales due to photon diffusion [19]. Unlike approaches inspired by general physical features, such as symmetries, intending to describe any given dataset, our “physics-informed” approach is highly specialized to the specific physics of this phenomenon, ensuring the output is interpretable and rooted in established physical principles.

This manuscript is organized as follows. Section II provides a concise review of genetic programming. In Sec. III, we explore the key physical effects that modify the linear matter power spectrum. In Sec. IV, we present our semi-analytical formulation of the matter transfer function, incorporating acoustic oscillations, and evaluate its performance. Then, in Sec. V, we make a contact of our formulation with observations by computing the two-point correlation function. Given the high interpretability of our formula for the oscillatory pattern, in Sec. VI we show how this formulation can be extended to scenarios involving massive neutrinos and modified gravity. Finally, we present our concluding remarks in Sec. VII.

II. GENETIC ALGORITHMS

Genetic programming is a machine learning paradigm that draws inspiration from biological evolution, employing principles akin to natural selection and “survival of the fittest” to address complex computational challenges. Within this framework, candidate solutions to a given problem evolve iteratively through generations, undergoing processes of selection, crossover, and mutation aimed at enhancing their fitness according to defined optimization criteria [8].

With its ability to evolve mathematical expressions and symbolic structures to fit data, GP offers a flexible and powerful approach to modeling relationships

between variables and parameters, or in other words, GP is a particularly well-suited tool for addressing symbolic regression problems. Now, we outline the application of genetic algorithms in SR problems in a concise manner. Initially, random mathematical expressions are generated to form the initial set of individuals. Subsequently, the fitness of each individual in the initial generation is assessed, often employing metrics such as mean squared error. Through a tournament selection process, a subset of the fittest individuals is chosen to proceed to the next generation. These selected individuals undergo genetic operations, typically involving crossover and mutation, to produce offspring. The subsequent generations consist of the most adept individuals from the previous iteration alongside their offspring, perpetuating the evolutionary cycle. This process iterates until an individual achieves the desired level of accuracy in describing the data. For further insights into the mechanisms and applications of GAs, interested readers can refer to Refs. [8, 20].

The adaptability of the GAs allows an effective navigation through complex function spaces and discovering of novel relationships, as it has been extensively witnessed across the physical sciences [21]. For instance, in quantum mechanics, GAs have proven effective in solving the Schrödinger equation for intricate systems [22]. In string theory, they contribute to the discovery of new Calabi-Yau manifolds [23]. Gravitational wave astronomy benefits from GAs by localizing and tracking strong gravitational events [24]. In condensed matter physics, GAs predict the final structure upon crystal formation [25]. Astrophysics employs GAs to optimize the search for astroparticles [26] and determine the mass of galaxy clusters [27]. Moreover, in cosmology, GAs serve various roles. They aid in constraining cosmological parameters from observational data [28–31], conducting null tests of cosmological datasets and the concordance model [32–35], and in forecast analyses [36]. Such methodologies are integral to relevant surveys like Euclid [37, 38].

III. THE MATTER POWER SPECTRUM

A. Overview

The Universe displays a remarkable homogeneity on scales exceeding 100 Mpc [39], yet it exhibits significant inhomogeneity on smaller scales. These variations correspond to structures formed by the successive collapse of matter confined within gravitational wells. This process of large-scale structure formation generates a statistical imprint, encapsulated in the matter power spectrum, denoted as $P(k)$.

In the absence of non-linear effects and warm or hot

dark matter, the scale-dependency of the matter power spectrum is given entirely in terms of the matter transfer function $T(k)$ as [11]

$$P(k) \propto k^{n_s} T^2(k), \quad (1)$$

where k denotes the wavenumber, conventionally measured in units of $[h/\text{Mpc}]$ with h representing the reduced Hubble constant, and n_s is the spectral index of primordial scalar fluctuations. This relation essentially describes how the initial density fluctuations (governed by the primordial power spectrum¹) evolve to form the structure in the universe, with the matter transfer function encoding the physics of its formation.

While the Cold Dark Matter (CDM) primarily drives the structure formation process, the inclusion of baryons introduces significant alterations to the CDM-only spectrum. Notably, as baryons are tightly coupled to photons prior to the recombination epoch, the pressure-induced oscillations observed in the angular power spectrum of the CMB also influence the matter power spectrum at intermediate scales [19]. Furthermore, this CDM+baryons landscape could be altered when factors like massive neutrinos, modifications to gravity, or the presence of dark energy are taken into account. Generally, the matter transfer function assumes a non-trivial time dependency, rendering Eq. (1) invalid. However, at a specific redshift, these modifications can once again be absorbed into $T(k)$. Massive neutrinos notably induce a suppression in the amplitude of $P(k)$ at smaller scales, typically observed for $k \gtrsim 0.6 h/\text{Mpc}$ [41]. On the other hand, the inclusion of dark energy or scenarios involving modified gravity impacts the growth of matter perturbations in two key ways: (i) by changing the rate of expansion of the universe, and (ii) by potentially acting as an effectively clustering component, further influencing the evolution of the overdensity field and thus shaping the matter power spectrum [42].

B. Calculation of Matter Power Spectra

During the process of structure formation, a variety of physical phenomena take place, making it exceedingly challenging to derive complete analytical solutions from the set of non-linear Einstein-Boltzmann equations. Nevertheless, efficient numerical solutions can be achieved using advanced Boltzmann solvers, as demonstrated by software packages such as CLASS [43]

and CAMB [44]. By default, these codes typically assume the concordance cosmological model. However, their architecture allows for easy incorporation of new models, such as those considering modified gravity or dark energy effects [45–49], as well as additional physical components like warm dark matter and interacting species [50].

The most accurate method for extracting theoretical insights about matter power spectra stems from large N -body simulations, such as the Quijote suite [51]. Nonetheless, a significant drawback of this approach is its substantial computational burden and limited adaptability to incorporate new models. Recent advancements have addressed the computational challenges by employing emulation techniques like neural networks or Gaussian processes to analyze $P(k)$ data from these simulations [52–55]. Although emulated matter power spectra offer high accuracy and rapid computation, it is worth noting that they suffer from the same limited adaptability which inherits from N -body simulations.

While deriving a complete analytical description of $P(k)$ from first principles remains unattainable, semi-analytical formulations have proven effective in approximating $P(k)$ [56, 57]. The widely utilized “analytical emulator” for the $P(k)$ of the concordance model is the Eisenstein-Hu (EH) formula, established around three decades ago [19].² The EH formula, rooted in well-understood physical phenomena, comprises approximately 30 expressions in its complete form, rendering it highly complex (see Appendix A).

However, it appears feasible to capture the typical “mountain” shape of the matter power spectrum using a simpler formulation. Pursuing this direction, two of the authors herein employed GAs to devise a semi-analytical representation of the de-wiggled $P(k)$ of Λ CDM. This formulation proves considerably simpler and slightly more precise than the de-wiggled EH formula [16]. Furthermore, the authors of the present work employed GAs to establish a parametric function for the de-wiggled $P(k)$ incorporating typical effects of modified gravity, demonstrating accuracy below 2% across all scales except within the band containing baryon acoustic oscillations (BAOs) (approximately $k = 0.05 h/\text{Mpc}$ and $k = 0.5 h/\text{Mpc}$) [17]. To the best of our knowledge, this $P(k)$ formulation for modified gravity represents the first semi-analytical formulation adaptable to a wide range of modified gravity scenarios, unlike other emulators restricted to specific models, such as Hu-Sawicki [59, 60] or DGP [61].

Semi-analytical formulations offer several advantages over machine learning emulators. While machine

¹ The primordial power spectrum is given by $P_R \equiv A_s (k/k_p)^{n_s - 1}$, where A_s is the amplitude of primordial scalar perturbations and k_p is an arbitrary pivot scale usually set at $k_p = 0.05 \text{ Mpc}^{-1}$ [40].

² Before the EH formula and Boltzmann solvers, the Bardeen-Bond-Kaiser-Szalay (BBKS) proposal was prevalent [58].

learning techniques often yield higher accuracy, semi-analytical formulations are simpler to incorporate into specific routines, devoid of installation prerequisites or wrappers for emulator usage. Additionally, as elaborated later, it's feasible to introduce physically motivated priors into the algorithm, constraining the search within the desired function space. This attribute enhances interpretability in the final formulation, in contrast to conventional black-box machine learning approaches.

C. The De-Wiggled Matter Power Spectrum

Because of the distinctive physical phenomena underlying the acoustic oscillations within the matter power spectrum, it becomes feasible to distinguish the BAO signal from the broad-band spectrum. As it is easier to explore small fluctuations on top of the full amplitude, we choose to write the matter transfer function as

$$T(k) \equiv T_{\text{nw}}(k) T_w(k), \quad (2)$$

where T_w encodes the acoustic oscillation pattern and T_{nw} denotes the broad-band (“no wiggles”) transfer function. Typically, the smooth T_{nw} is found after applying a “de-wiggle” process to the linear power spectrum, or equivalently, to the linear transfer function. Different methodologies have been applied in the literature, but the predominant approaches include using the zero-baryon case of the EH formula [19], or employing filters for signal processing [62], such as the Savitzky-Golay filter [63].

In Ref. [16], two of the herein authors introduced a semi-analytical formulation for the de-wiggled matter transfer function of Λ CDM using GAs. The formula is given by

$$T_{\text{nw}}(x) = [1 + 59.0998 x^{1.49177} + 4658.01 x^{4.02755} + 3170.79 x^{6.06} + 150.089 x^{7.28478}]^{-1/4}, \quad (3)$$

where x is a dimensionless variable defined as

$$x(k; \omega_b, \omega_m) \equiv \left(\frac{k}{\omega_m - \omega_b} \right) \frac{\text{Mpc}}{h}, \quad (4)$$

with k in units of [h/Mpc]. This simple formula proves to be slightly more accurate than the considerably more complex de-wiggled EH formulation when compared with the full matter transfer function retrieved from CLASS, where most errors stem from neglecting the BAO signal in the formulation of $T(k)$.

D. Wiggles in the Matter Transfer Function

Once a de-wiggle process has been selected, the BAO signal can be isolated by dividing the full $P(k)$

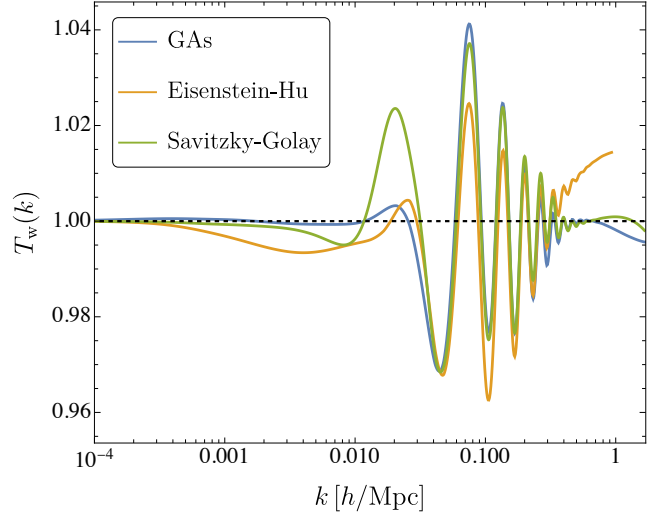


FIG. 1. (Color online) Comparison of the BAO signals extracted from the matter transfer function using the zero-baryon case of the EH formula (yellow line), the no-wiggles $T_{\text{nw}}(k)$ in Eq. (3) (blue line), and the Savitzky-Golay filter (green line).

by the de-wiggled $P_{\text{nw}}(k)$. However, the specific de-wiggle method can yield to different fits for the BAO signal [64]. In Fig. 1, we show that the EH formula, the GA formula in Eq. (3), and the Savitzky-Golay filter, indeed yield to different acoustic oscillations patterns. Notably, the most prominent effect is a change in the amplitude of the wiggles, while their positions remains relatively unaltered.

Given that acoustic oscillations possesses a physical meaning, and since the BAO signal isolation depends on the de-wiggle process, it is clear that each oscillation pattern will inherit errors from the de-wiggle and will contain spurious physics, as it can be noted from the differences between patterns at the largest and smallest scales.

Although an exact formulation for the wiggles is unattainable, it is quite possible to describe the physical phenomena behind it. In the following, we will consider some of the most relevant physical effects underlying the acoustic oscillations in the matter power spectrum.

In Ref. [19], Eisenstein and Hu propose a formulation for $T(k)$ involving all the relevant physical effects, acoustic oscillations, Compton drag, velocity overshoot, baryon infall, Silk damping, and CDM growth suppression. In general, this formula has two parts: one associated to the CDM, and one when the effects of baryons are taken into account. Baryons produce several relevant effects on $T(k)$. *i*) Since baryons are tightly coupled with the photons in the primordial universe prior to recombination, the pressure-induced oscillations seen

in the CMB are also inherited by the matter power spectrum, but with a reduced amplitude. This corresponds to the BAO signal. *ii)* When baryons and photons decouple, photon diffusion occurs and acoustic oscillations are exponentially damped, this is known as Silk effect. *iii)* Baryons are dragged by gravitational wells sourced by CDM and start to cluster into the CDM haloes. This produce a further suppression at smaller scales.

In the next section, we will use this physical information to build a template function in order to facilitate the random search of our genetic algorithm.

ical symmetries found in well-known laws of physics, such as symmetry under rotation, translations, etc, aiming at finding the correct formula describing the dataset [5, 6]. Our methodology, instead, specialized in a particular phenomenon and lacks this general purpose of finding the formula for any given dataset. Therefore, our “physics-informed” approach enhances the interpretability of the algorithm’s output, as opposed to a purely random function combination. Furthermore, this strategy enables the identification of potential gaps in the current understanding of the particular phenomenon under scrutiny, like the oscillatory pattern in the matter power spectrum.

IV. GENETIC ALGORITHMS EMULATOR FOR $P(k)$

A. Physics-Informed Approach to Genetic Programming

In accordance with the preceding discussion, the origin and evolution of the acoustic oscillation pattern observed in the matter power spectrum stem from established physical phenomena. The EH formula effectively consolidates these effects into a semi-analytical expression for the matter transfer function, thus unifying diverse physical phenomena occurring across various scales. Our aim is to incorporate the understanding of these underlying physical effects into our GA.

In the context of the cosmological inference problem, the parameter space of a given model is sampled to identify the parameter set that best aligns with data. In a typical Markov chain Monte Carlo run, the random search initiates from a predefined point, and the search space is delimited by previous knowledge gathered about the parameter space, which is encoded in the so-called priors. Resembling the MCMC methodology applied to the parameter space of a model, the GAs conduct a stochastic exploration in the model space of a given phenomenon instead. This model space is determined by a defined grammar set composed by some operations (e.g., addition, product, etc), and functions (e.g., exponential, logarithm, trigonometric, hyper-geometric, etc). Following this analogy, we may add physically well-motivated priors to our GA to delimit its search. In this particular case, we can take advantage of our knowledge about the underlying physics governing the BAO pattern in $P(k)$ to propose a template in order to focus the search of our GA.

This methodology, in particular, differs from other approaches integrating “physics-inspired” knowledge into its search algorithm. As a particular example, the **AI-Feynman** code seeks in the provided dataset for typ-

B. BAO Signal Template for the GAs

Here, we assume that the broad band matter transfer function is given by our previous GAs formulation in Eq. (3). We further anticipate that the oscillating pattern will encompass the following effects:

1. A sinusoidal function representing oscillations occurring below the sound horizon.
2. An exponential damping factor to account for the effects of photon diffusion at scales below the sound horizon.
3. An amplitude suppression term to characterize the asymptotic behavior of the acoustic oscillations.

These considerations are encapsulated in the following template:

$$T(k; \omega_b, \omega_m) \equiv T_{\text{nw}} [1 + f_{\text{amp}} e^{-f_{\text{Silk}}} \sin(f_{\text{osc}})]. \quad (5)$$

Now, the problem is translated into finding suitable analytical forms for the amplitude suppression function f_{amp} , the Silk damping function f_{Silk} , and the oscillatory pattern function f_{osc} .³ We derive inspiration from the EH formulation, where the oscillatory behavior of the matter transfer function is encoded in the baryon transfer function, given by:

$$T_b = \left[\frac{\tilde{T}_0(k; 1, 1)}{1 + (k s / 5.2)^2} + \frac{\alpha_b}{1 + (\beta_b / k s)^3} e^{-\left(\frac{k}{k_{\text{Silk}}}\right)^{1.4}} \right] j_0(k \tilde{s}), \quad (6)$$

In Appendix A, we can see that the complexity arising from the various terms involved in T_b , such as α_b , β_b , \tilde{s} . However, a closer examination of these terms reveals

³ Note here the symbol f denotes a function estimated by the GA and is not a frequency.

Constant	Value	Constant	Value	Constant	Value
c_1	0.00785436	c_2	0.177084	c_3	0.00912388
c_4	0.618711	c_5	11.9611	c_6	2.81343
c_7	0.784719				
a_1	1.43679	a_2	2.86538	a_3	0.949946
a_4	0.746495	a_5	1.2384	a_6	3.49433
a_7	0.311833	a_8	0.19012	a_9	0.233442
a_{10}	0.614879	a_{11}	0.0532925	a_{12}	1.38231
a_{13}	1.34703	a_{14}	31.7525	a_{15}	1.22438
a_{16}	57.7364	a_{17}	1.04748	a_{18}	0.102231
a_{19}	0.999364				

TABLE I. Best-fit parameters c_i for the sound horizon s_{GA} [65], and a_i for the matter transfer function $T(k)$ in Eq. (10).

that they can be approximated by simple functions. For instance, we have determined that α_b and β_b , as given in Eq. (A11) and (A12), can be approximated by

$$\alpha_b \approx 0.131173 - 0.209954 \omega_b^{0.157385} + 0.186002 \omega_m, \quad (7)$$

$$\beta_b \approx 1.68668 - 30.2817 \omega_b + 47.4275 \omega_m, \quad (8)$$

with an accuracy of 0.02% and 0.007%, respectively, in the ranges $\omega_b \in [0.0214, 0.0234]$ and $\omega_m \in [0.13, 0.15]$, which are around 10σ from the best-fit values found by

the Planck Collaboration [40]. The term \tilde{s} determines the shifting of the first acoustic peaks:

$$\tilde{s} = s \left[1 + \left(\frac{\beta_{\text{node}}}{k s} \right)^3 \right]^{-1/3}, \quad (9)$$

where β_{node} is a simple function solely dependent on ω_m [see Eq. (A15)].

Having considered the preceding discussion, we propose the following template for the matter transfer function:

$$T_{\text{GA}}(k; \omega_b, \omega_m) \equiv T_{\text{nw}}(k) \left[1 + \frac{f_{\alpha}(\omega_b, \omega_m)}{a_1 + \{f_{\beta}(\omega_b, \omega_m)/(ks_{\text{GA}})\}^{a_2}} e^{-(k/k_{\text{Silk}})^{a_3}} \sin \left\{ \frac{a_4 k s_{\text{GA}}}{(a_5 + \{f_{\text{node}}(\omega_m)/(ks_{\text{GA}})^{a_6}\})^{a_7}} \right\} \right], \quad (10)$$

where we have replaced the sound horizon s given in Ref. [19] [see Eq. (A13)] with the more accurate expression derived from GAs [65]

$$s_{\text{GA}} \equiv \frac{1}{c_1 \omega_b^{c_2} + c_3 \omega_m^{c_4} + c_5 \omega_b^{c_6} \omega_m^{c_7}}, \quad (11)$$

where c_i , $i = 1, \dots, 7$ are constants given in Table I. The Silk damping scale (in units of [1/Mpc]) is given by Eq. (A9) as

$$k_{\text{Silk}} \equiv 1.6 \omega_b^{0.52} \omega_m^{0.73} \{1 + (10.4 \omega_m)^{-0.95}\}. \quad (12)$$

The functions in Eq. (5) are replaced by

$$f_{\text{amp}} \equiv \frac{f_{\alpha}(\omega_b, \omega_m)}{a_1 + \{f_{\beta}(\omega_b, \omega_m)/(ks_{\text{GA}})\}^{a_2}}, \quad (13)$$

$$f_{\text{Silk}} \equiv (k/k_{\text{Silk}})^{a_3}, \quad (14)$$

$$f_{\text{osc}} \equiv \frac{a_4 k s_{\text{GA}}}{(a_5 + \{f_{\text{node}}(\omega_m)/(ks_{\text{GA}})^{a_6}\})^{a_7}}, \quad (15)$$

where a_i , $i = 1, \dots, 7$ are constants to be optimized by the genetic algorithm in each generation. The functions f_{α} , f_{β} , and f_{node} are simple power law functions of ω_b and ω_m , which will be determined by the GA.

The goodness of fit of our GA expression $T_{\text{GA}}(k)$ is

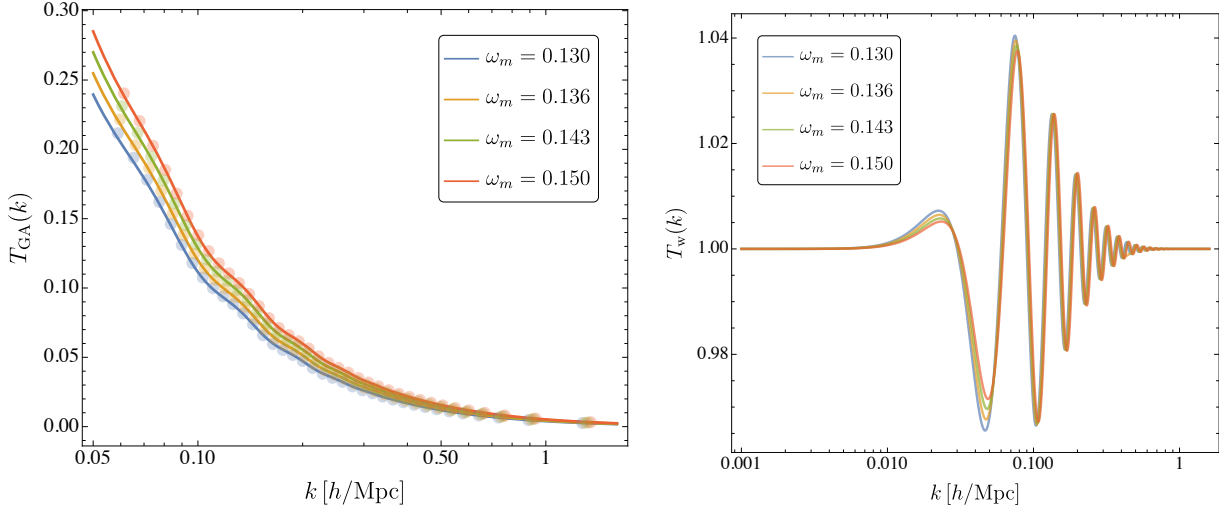


FIG. 2. Left: the plots illustrate the fitting of the GA formula in Eq. (10) (solid lines) against data obtained from **CLASS** (points). In these examples, we fix $\omega_b = 0.02273$ and vary ω_m . The agreement between our formulation and the **CLASS** data is remarkable. Right: The BAO signal, expressed as $T_{\text{GA}}(k)/T_{\text{nw}}(k)$, is shown. It is seen that increasing ω_m leads to a further suppression of the peaks and shifts them to smaller scales. However, the Silk damping appears to be relatively unaffected by variations in ω_m .

quantified as

$$\% \text{Acc} = \frac{100}{N} \sum_{i=1}^N \left| \frac{T_{i,\text{CLASS}} - T_{i,\text{GA}}}{T_{i,\text{CLASS}}} \right|, \quad (16)$$

where N is the number of data points $\{k_i, T_{\text{CLASS}}(k_i)\}$ retrieved from **CLASS**, and the subindex i is a shorthand notation for equivalent to $T_i \equiv T(k_i)$. Here, we considered 4×4 pairs of parameters $\{\omega_b, \omega_m\}$ varying in the ranges $\omega_b \in [0.0214, 0.0234]$, and $\omega_m \in [0.13, 0.15]$, which are around 10σ from the best-fit values found by the Planck Collaboration [40]. Then, after few thousand generations, the genetic algorithm converged to the following functions:

$$f_\alpha(\omega_b, \omega_m) \equiv a_8 - a_9 \omega_b^{a_{10}} + a_{11} \omega_m^{a_{12}}, \quad (17)$$

$$f_\beta(\omega_b, \omega_m) \equiv a_{13} - a_{14} \omega_b^{a_{15}} + a_{16} \omega_m^{a_{17}}, \quad (18)$$

$$f_{\text{node}}(\omega_m) \equiv a_{18} \omega_m^{a_{19}}. \quad (19)$$

All the constants are given in Table I.

C. Performance

Here, we evaluate the performance of the novel formulation for the matter transfer function, denoted by $T_{\text{GA}}(k)$, as defined in Equation (10), utilizing the computational output generated from **CLASS**.

Firstly, we perform a qualitative evaluation of the fit in Fig. 2. We can see that for fixed ω_b and variable ω_m , the fit exhibits exceptional agreement. In fact, the final

accuracy of Eq. (10), as measured by Eq. (16), is 0.347% using $N = 1824$ data points. In the right panel of this figure, the BAO signal extracted as $T_{\text{GA}}(k)/T_{\text{nw}}(k)$ is depicted. Notable effects of the variation in ω_m on the BAO signal are discernible. For instance, an increasing ω_m leads to a further suppression of the amplitude of the peaks, which is encoded in f_{amp} . Additionally, this increment in ω_m results in a slight shift of the peaks position toward smaller scales. This phenomenon is elucidated in Ref. [19] as follows. For $ks \lesssim \beta_{\text{node}}$, we have $\tilde{s} \approx ks^2/\beta_{\text{node}} < s$. Since β_{node} is proportional to a power of ω_m , thus an increase in ω_m shifts the nodes to higher k values, i.e., to smaller scales.

In the left panel of Fig. 3, we depict the percentage accuracy of both the EH formula and our new GA formulation as functions of k , utilizing the best-fit parameters from Planck: $\omega_b = 0.0224$ and $\omega_m = 0.1448$ [40]. Notably, the accuracy of the GA formula (red line) remains below 0.5% for both larger scales ($k \lesssim 0.02$ [h/Mpc]) and smaller scales ($k \gtrsim 0.2$ [h/Mpc]). This indicates that our GA formulation accurately captures the behavior above the sound horizon and below the Silk damping scale. However, the accuracy slightly diminishes to approximately 1%-1.5% on intermediate scales, where the first acoustic peaks are observed (as depicted in the right panel of Fig. 2). Nevertheless, this deviation does not significantly impact our formulation, given that this level of accuracy falls within the expected range for ongoing/future observational missions. Moreover, owing to the high interpretability of our formulation, we have the flexibility to enhance it by incorporating additional

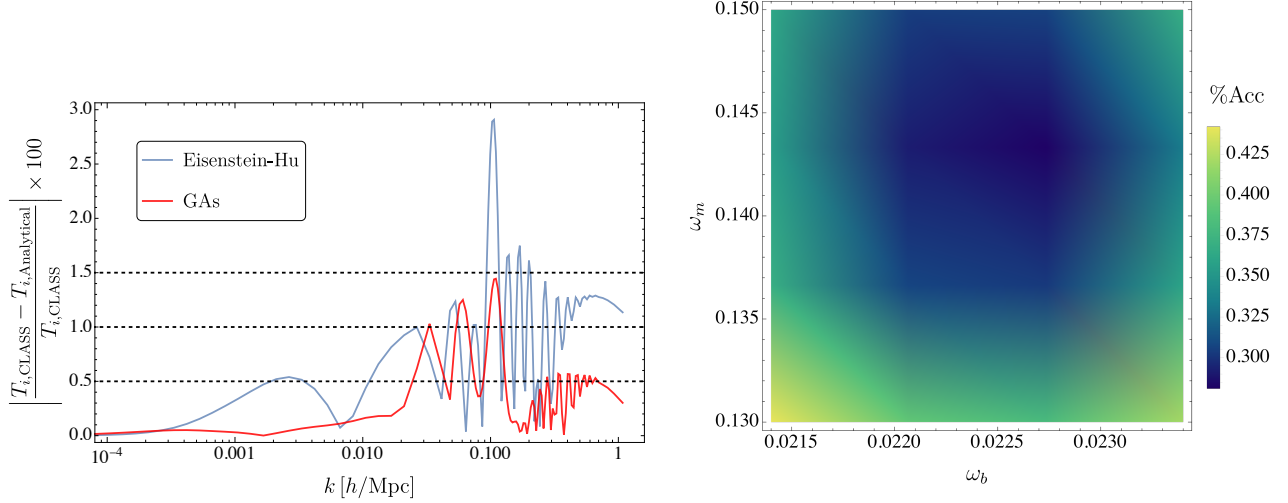


FIG. 3. (Color online) Left: accuracy of the EH (blue line), and the GA (red line) fitting formulae as a function of the scale k and fixed $\{\omega_m, \omega_b\}$. The parameters for these plots are: $\omega_b = 0.0224$, and $\omega_m = 0.1448$, which correspond to the best-fit parameters from Planck [40]. For the larger scales and smaller scales ($k < 0.02$ [h/Mpc] and $k > 0.2$ [h/Mpc]), the accuracy of the GA formulation are below 0.5%. However, on the intermediate scales where the first peaks are found, the accuracy drops until some 1.5% for same values. Right: average accuracy of the GA fitting formula for all k as a function of $\{\omega_m, \omega_b\}$. As it can be seen, the formula is always below 0.5% accurate in overall.

terms to accommodate possible missing physical effects or by considering more intricate functions to describe the position and amplitude of these first peaks, which we prefer not to do in order to keep the simplicity of our formulation. On the other hand, in the right panel of Fig. 3, a density plot illustrates the overall accuracy across all scales while varying the parameters ω_b and ω_m . It is clear that our new GA formulation of the matter transfer function consistently provides a highly accurate description, always maintaining an accuracy below 0.5% overall.

V. CONTACT WITH OBSERVATIONS: THE BAO SCALE

While the matter power spectrum is a fundamental quantity in cosmology, it serves as a summary statistic. The primary observable in large-scale structure surveys is the two-point correlation function (2PCF), which measures clustering at various spatial scales. The 2PCF is defined as:

$$\xi(\mathbf{r}) \equiv \langle \delta(\mathbf{x})\delta(\mathbf{x} + \mathbf{r}) \rangle, \quad (20)$$

where $\delta(\mathbf{r})$ represents the density fluctuation at position \mathbf{x} . The 2PCF quantifies the correlation between density perturbations at two points separated by \mathbf{r} , thereby providing insight into the strength of structure on different scales [11]. Indeed, the matter power spectrum can be

expressed as the Fourier transform of the 2PCF

$$\xi(\mathbf{r}) \equiv \frac{1}{(2\pi)^3} \int d^3k P(\mathbf{k}) e^{-i\mathbf{k}\cdot\mathbf{r}}. \quad (21)$$

In this section, we compute the 2PCF using P_{GA} and compare it to results obtained through conventional methods involving a Boltzmann solver and the EH formula.

For large-scale structure surveys (e.g., SDSS), the observed matter power spectrum P_{obs} is modeled as [66, 67]

$$P_{\text{obs}}(k; \mu) \equiv C(k) P_{\text{nw}} [1 + (O_{\text{lin}} - 1) e^{-k^2 \Sigma_{\text{nl}}^2 / 2}], \quad (22)$$

where $C(k)$ is a coefficient encoding the effects due to redshift-space distortions given by⁴

$$C(k; \mu, \Sigma_s) \equiv \frac{[\sigma_8 b + f\sigma_8(1 - S(k))\mu^2]^2}{(1 + k^2\mu^2\Sigma_s^2/2)}. \quad (23)$$

In the previous expressions, σ_8 is the variance of matter fluctuations on a scale of $R = 8 \text{ Mpc}/h$, b is the linear bias, $f\sigma_8$ is the growth rate, $S(k) \equiv \exp(-k^2\Sigma_r^2/2)$ is the smoothing applied during the reconstruction process with $\Sigma_r \equiv 15 \text{ Mpc}/h$, μ is the cosine of the angle

⁴ We ignore the Alcock-Paciński effect since we compute the matter power spectrum at $z = 0$.

between the line-of-sight and the wavevector \mathbf{k} , Σ_s is a parameter quantifying the random motion of galaxies within clusters, P_{nw} is the de-wiggled linear matter power spectrum, O_{lin} is defined as

$$O_{\text{lin}} \equiv P_{\text{lin}}/P_{\text{nw}}, \quad (24)$$

where P_{lin} is the linear matter power spectrum typically computed using a Boltzmann solver. Following this definition, O_{lin} encodes the oscillatory pattern due to the BAOs. This oscillatory pattern is multiplied by a Gaussian distribution with

$$\Sigma_{\text{nl}}^2(\mu) \equiv \frac{2}{3}\Sigma_{xy}^2 + \frac{1}{3}\Sigma_z^2, \quad (25)$$

$$\Sigma_{xy} \equiv \sigma_8 \int \frac{dk}{2\pi^2} k P_{\text{lin}}(k), \quad (26)$$

$$\Sigma_z \equiv (1 + f\sigma_8)\Sigma_{xy}. \quad (27)$$

Finally, given $P_{\text{obs}}(k; \mu)$ we determine the multipole moments as

$$P_\ell(k) = \frac{2\ell+1}{2} \int d\mu P_{\text{obs}}(k; \mu) L_\ell(\mu), \quad (28)$$

where L_ℓ is the Legendre polynomial of order ℓ . These moments are transformed to the 2PCF moments via:

$$\xi_\ell(r) = \frac{i^\ell}{2\pi^2} \int dk k^2 P_\ell(k) j_\ell(kr), \quad (29)$$

where j_ℓ is the spherical Bessel function of order ℓ .

Typically, the term encoding the BAO signal, O_{lin} , is computed using a Boltzmann solver to obtain P_{lin} , and a de-wiggled power spectrum given by the EH formula or by a signal filter like the Savitzky-Golay filter. In contrast, our GAs formulation provides this term directly in Eq. (10) as $O_{\text{lin}} = T_w^2(k)$, with P_{nw} related to $T_{\text{nw}}(k)$ in Eq. (3). As demonstrated in Ref. [64], different de-wiggling processes can produce varying BAO templates.

Figure 4 compares the BAO templates derived from the monopoles $r^2\xi_0$ using using **CLASS** in conjunction with the de-wiggled EH spectrum (dashed lines) versus those obtained solely from GAs (solid lines) for fixed $\omega_b = 0.02206$ and $\omega_m = 0.130$ and $\omega_m = 0.150$. The bias is set to $b = 1$ at $z = 0$, with other parameters such as σ_8 and $f\sigma_8$ directly retrieved from **CLASS**. This figure illustrates that for both formulations, increasing matter shifts the BAO peak to smaller scales, as expected. However, the BAO peak positions predicted by both methods differ, as highlighted by the vertical lines. This difference in the peaks positions, which is around 2 Mpc/h for both cases, is due merely to the difference in the procedure. A more rigorous treatment of the 2PCF, and a detailed comparison with real data from large-scale structure surveys, such as SDSS, would be interesting but is beyond the scope of this work and is reserved for future research.

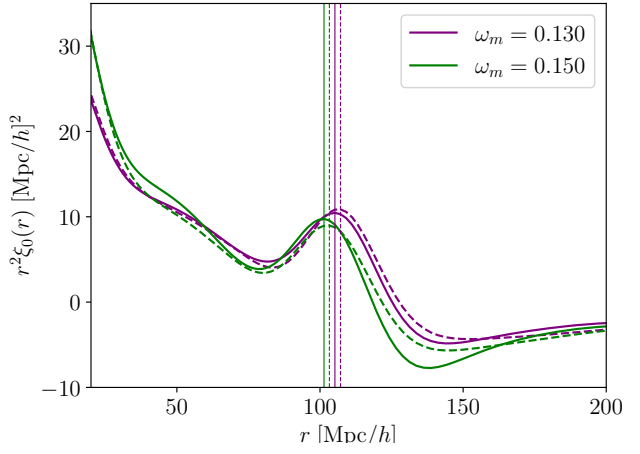


FIG. 4. (Color online) Comparison between the BAO template computed using **CLASS** in conjunction with the de-wiggled EH formula (dashed lines), and the matter power spectrum retrieved from GAs solely (solid lines), for fixed $\omega_b = 0.02206$ and $\omega_m = 0.13$ and $\omega_m = 0.15$. While both methods yield similar results, the BAO peak positions differ slightly, indicated by the vertical lines for each ω_m value, approximately by 2 Mpc/h in both cases. A more rigorous treatment of the 2PCF and a detailed comparison with observational data is deferred to future work.

VI. EXTENSION TO OTHER SCENARIOS

One of the most compelling aspects of our “physics-informed” approach to the symbolic regression problem is the high interpretability of the resulting expressions. In the following sections, we will demonstrate how our formula for the BAO signal, encapsulated in $T_w(k)$, can be extended to scenarios beyond the standard Λ CDM model.

A. Massive Neutrinos

It is well-known that massive neutrinos can alter the matter power spectrum at small scales. However, their impact on the BAO signal is minimal, allowing us to adapt our formula to this scenario as a first approximation. In Ref. [16], we presented a GA-derived expression for the de-wiggled matter transfer function incorporating one massive neutrino:

$$T_{\text{nw}}^{(\nu)}(y) = [1 + 56.4933y^{1.48261} + 3559.23y^{3.76407} + 4982.44y^{5.68246} + 374.167y^{7.14558}]^{-1/4}, \quad (30)$$

where y is a dimensionless variable defined as

$$y(k; \omega_b, \omega_m, \omega_\nu) \equiv \left(\frac{k}{\omega_m - \omega_b + \omega_\nu} \right) \frac{\text{Mpc}}{h}, \quad (31)$$

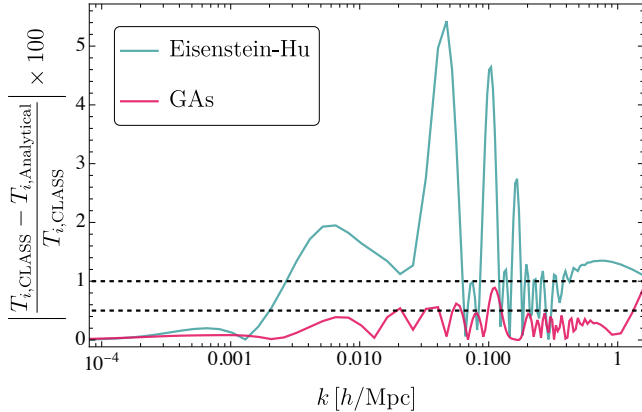


FIG. 5. (Color online) Accuracy comparison of the EH (cyan line) and GA (fuchsia line) fitting formulae as a function of the scale k , with fixed parameters: $\omega_b = 0.0214$, $\omega_m = 0.136$, and $\omega_\nu = 0.00107$. Our formulation demonstrates an excellent agreement with the data from **CLASS**, reproducing the matter transfer function with an accuracy better than 1% across all relevant scales, thereby significantly improving upon the EH formulation.

with k in units of $[h/\text{Mpc}]$, and ω_ν representing the reduced density parameter of neutrinos. This formula shows an average accuracy of 0.99%, when compared with data from **CLASS**, for its parameters ω_b and ω_m in the same ranges as in Sec. IV B, and the mass of neutrinos in the range $0.06 \text{ eV} \leq \sum m_\nu \leq 0.12 \text{ eV}$, with the corresponding reduced density calculated as $\omega_\nu \equiv 0.0107(\sum_\nu m_\nu/1.0 \text{ eV})$.

In Fig. 5, we compare the matter transfer function from Eisenstein and Hu [68] with our new formulation, which includes the de-wiggled transfer function from Eq. (30) and the term in squared brackets in Eq. (10):

$$T_{\text{GA}}^{(\nu)} \equiv T_{\text{nw}}^{(\nu)}(k, \omega_b, \omega_m, \omega_\nu) T_{\text{w}}(k, \omega_b, \omega_m). \quad (32)$$

For this comparison, we set the parameters $\omega_b = 0.0214$, $\omega_m = 0.136$, and $\omega_\nu = 0.00107$. Our formulation achieves a description of the **CLASS** data with better than 1% accuracy across all relevant scales, representing an improvement over the EH formulation. It is important to note that the EH formulation, while it considers the presence of massive neutrinos, does not account for the oscillatory effects induced by baryon pressure. Consequently, a transfer function incorporating acoustic oscillations is not provided in their work. In this context, our proposed formulation is the first to address this gap by including both the effects of massive neutrinos and baryon acoustic oscillations in the transfer function.

B. Modified Gravity

The adaptability of the wiggle pattern $T_{\text{w}}(k)$ to the de-wiggled transfer function $T_{\text{nw}}^{(\nu)}$ was anticipated, given that massive neutrinos further suppress the amplitude of $P(k)$ at scales $k \gtrsim 0.6 h/\text{Mpc}$ [41]. Therefore, this suppression effect should be accurately captured by the de-wiggled transfer function $T_{\text{nw}}^{(\nu)}$, with minimal impact on the acoustic oscillatory pattern. Similarly, the effects on $P(k)$ due to modifications of gravity are more significant at the largest or smallest scales. Thus, we expect that the oscillatory pattern in the $P(k)$ of viable modified gravity theories should not deviate substantially from the ΛCDM archetype, which is accurately described by our $T_{\text{w}}(k)$.

In Ref. [17], the authors demonstrated the feasibility of extending the de-wiggled matter transfer function in Eq. (3), originally valid only for ΛCDM , to account for general cosmological effects introduced by covariant modifications of gravity. This formulation exhibits approximately 1%-2% mean accuracy when compared with the full $P(k)$ of various models in **hi-class** [48] and **mg-class** [49]. The primary source of error arises from the exclusion of the BAO signal. Nevertheless, to the best of our knowledge, this represents the only available formulation for the broad-band linear power spectrum for modified gravity theories.

This broad-band power spectrum for the $P(k)$ of modified gravity theories is given by:

$$P_{\text{nw}}^{(\text{MG})}(k) \equiv [1 - \sigma(k; k_0, \beta)] P_{\text{large}}(k; s, n_s) + \sigma(k; k_0, \beta) P_{\text{small}}(k; \alpha, \omega_b, \omega_m). \quad (33)$$

where P_{large} encodes the effects at the largest scales, while P_{small} encodes the effects on the smallest scales. These functions are respectively given by

$$P_{\text{large}}(k; s, n_s) \equiv A(s) \left(\frac{k}{h/\text{Mpc}} \right)^{n_s} [(Mpc/h)^3], \quad (34)$$

$$A(s) \approx 3 \times 10^6 (1 + s), \quad (35)$$

$$P_{\text{small}}(k; \alpha, \omega_b, \omega_m) = 2.52395 \times 10^6 \left(\frac{k}{h/\text{Mpc}} \right)^{0.96452} \times (1 + 0.710636\alpha^3 + 1.88019\alpha^4 + 0.939217\alpha^5) \times T_{\text{nw}}^2(k, \omega_b, \omega_m) [(Mpc/h)^3]. \quad (36)$$

These separated descriptions are linked through the “transition” function:

$$\sigma(k; k_0, \beta) = \left[1 + e^{-(\ln k - \ln k_0)/\beta} \right]^{-1}. \quad (37)$$

This formulation requires to find the extra parameters: the shift s at large scales, the overall enhancement (or

suppression) parameter α , the transition center k_0 , and the transition width β switching between P_{large} and P_{small} . See Ref. [17] for further details about this formula.

Therefore a complete description of the matter power spectrum, i.e., broad-band plus acoustic oscillations, will be of the form

$$P_{\text{GA}}^{(\text{MG})}(k) \equiv P_{\text{nw}}^{(\text{MG})}(k) T_{\text{nw}}^2(k). \quad (38)$$

In Fig. 6, we evaluate the accuracy of our formula in Eq. (38) against data retrieved from `CLASS`. We choose the model `plk_late` to do this comparison, since it is already implemented in `mg_class`, and it has been used as modified gravity model template by observational collaborations such as Planck [69] and DES [70]. In this model, the slip parameters, which measure deviations from GR, are proportional to the density parameter of “effective” dark energy Ω_{DE} through the constants E_{ii} [49]. Within our framework, we translate the parameters of the modified gravity model, i.e., the parameters E_{ii} , into the parameters of our GAs formulation, i.e., α , β , k_0 , and s in Eq. (33). This parameters can be found by using a simple minimization process which guarantees that our formula accurately reproduce the given model. As it can be seen in this figure, our formula describes the $P(k)$ within 1% accuracy for the largest and smallest scales, for all the parameters considered here. We also note a drop in the accuracy up to 2% for intermediate scales, which again, is within the error managed by current and future large-scale structure surveys.

VII. CONCLUSIONS AND OUTLOOKS

The matter power spectrum, $P(k)$, is a crucial summary statistics in cosmology, bridging theoretical predictions with observational data from large-scale structure surveys. Due to the complexity of the Einstein-Boltzmann equations, which govern the growth of the matter density field, analytical solutions for $P(k)$ are unattainable. Typically, $P(k)$ is computed using sophisticated numerical integrators, known as Boltzmann solvers, or derived from large N -body simulations.

To accelerate the computation of $P(k)$, various machine learning-based emulators have been developed. However, these emulators require large datasets for training, limiting their applicability across diverse models. For most practical applications, where extreme precision is not essential, analytical descriptions of $P(k)$ that capture the essential information are preferable.

For the ΛCDM model, the Eisenstein-Hu (EH) formula has provided an analytical solution for about 30 years, albeit a complex one due. Previously, two of the authors herein introduced a simplified formula for the

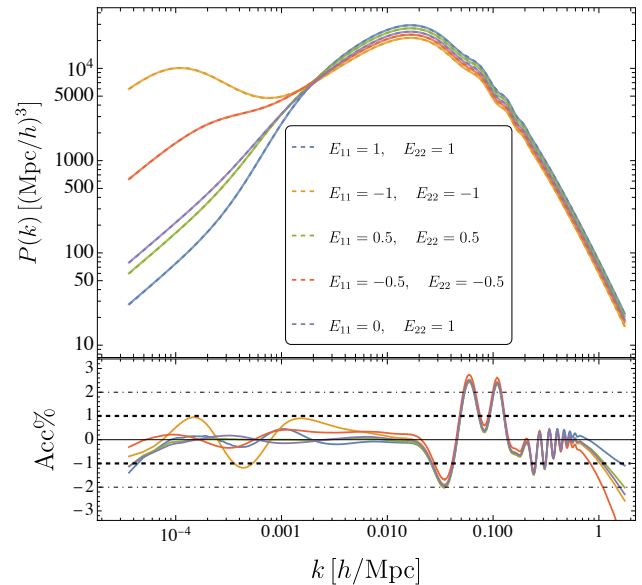


FIG. 6. Performance of the full analytical formulation of the $P(k)$ considering modified gravity effects in Eq. (38) against data retrieved from `mg_class`. The chosen model for the comparison is the `plk_late`, in which the slip parameters are proportional to the density parameter of dark energy, with proportionality constants E_{ii} . We see that our formula reproduce the `mg_class` data 1% accurate for the largest and smallest scales, with a drop of accuracy to some 2% for the intermediate scales, again, where the first peaks of the acoustic pattern are located.

“de-wiggled” linear matter transfer function, which is slightly more accurate than the zero-baryon case of the EH formula and significantly simpler.

In this work, we extend that formulation to include the characteristic wiggling pattern caused by baryon acoustic oscillations (BAO). Our new formula, derived using a “physics-informed” genetic algorithm, incorporates three main effects: *i*) a sinusoidal behavior below the sound horizon, *ii*) suppression by baryon drag, and *iii*) further exponential suppression at smaller scales due to photon diffusion. The resulting formula, presented in Eq. (10), achieves below 1% accuracy for almost all relevant scales and is simpler and more accurate than the EH formula.

Observations and theory are connected through the two-point correlation function (2PCF) $\xi(r)$, which can be derived from the matter power spectrum. Typically, the 2PCF is calculated using a Boltzmann solver to obtain the linear matter power spectrum P_{lin} and a de-wiggled matter power spectrum for P_{nw} , such as that provided by the Eisenstein-Hu (EH) formula. In this study, we compared the results for the BAO template $r^2\xi_0(r)$ computed using the conventional method,

specifically CLASS combined with the de-wiggled EH formula, against those obtained using our Genetic Algorithm (GA) formulation. Our findings reveal that both approaches produce similar BAO templates; however, the BAO peaks are observed at slightly different scales. This discrepancy suggests variations in the “standard ruler” predicted by each method, which is crucial for precise cosmological measurements.

The interpretability of our formulation, grounded in established physical principles, enabled us to extend it to account for the effects of massive neutrinos and modifications of gravity. These extensions maintain high accuracy and represent pioneering advancements in the field. To further demonstrate the utility of our analytical formulas, we aim to use these GA formulations to evaluate the impact of massive neutrinos and modified gravity on the characteristic scale of the BAO signal by computing the corresponding two-point correlation functions. Additionally, we plan to compare these BAO templates with real observational data to constrain the parameters of the models under consideration. However, we reserve this intriguing project for future work.

ACKNOWLEDGEMENTS

BOQ would like to express his gratitude to the Facultad de Ciencias Físicas y Matemáticas of Universidad de Chile for their hospitality during the completion of this work. BOQ is supported by Patrimonio Autónomo - Fondo Nacional de Financiamiento para la Ciencia, la Tecnología y la Innovación Francisco José de Caldas (MIN- CIENCIAS - COLOMBIA) Grant No. 110685269447 RC-80740-465-2020, project 69723 and by Vicerrectoría de Investigaciones - Universidad del Valle Grant No. 71357. DS acknowledges financial support from the Fondecyt Regular project number 1200171. SN acknowledges support from the research project PID2021-123012NB-C43 and the Spanish Research Agency (Agencia Estatal de Investigación) through the Grant IFT Centro de Excelencia Severo Ochoa No CEX2020-001007-S, funded by MCIN/AEI/10.13039/501100011033.

Numerical Codes

All the codes used in this work are publicly available in the GitHub profile of the author JBOQ: <https://github.com/BayronO> in the folder `Wiggles-in-Tk`.

Appendix A: EH Formula

The transfer function given by Eisenstein and Hu [19] has the following form:

$$T(k) = \frac{\Omega_b}{\Omega_0} T_b(k) + \frac{\Omega_c}{\Omega_0} T_c(k), \quad (A1)$$

where $\Omega_0 = \Omega_b + \Omega_c$. The terms involved in this formula are the following:

$$T_b = \left[\frac{\tilde{T}_0(k; 1, 1)}{1 + (ks/5.2)^2} + \frac{\alpha_b}{1 + (\beta_b/ks)^3} e^{-\left(\frac{k}{k_{\text{Silk}}}\right)^{1.4}} \right] j_0(k\tilde{s}), \quad (A2)$$

$$T_c = f\tilde{T}_0(k, 1, \beta_c) + (1 - f)\tilde{T}_0(k, \alpha_c, \beta_c), \quad (A3)$$

$$\tilde{T}_0(k, \alpha_c, \beta_c) = \frac{\ln(e + 1.8\beta_c q)}{\ln(e + 1.8\beta_c q) + Cq^2}, \quad (A4)$$

$$f = \frac{1}{1 + (ks/5.4)^4}, \quad (A5)$$

$$C = \frac{14.2}{\alpha_c} + \frac{386}{1 + 69.9q^{1.08}}, \quad (A6)$$

$$q = \frac{k}{13.41k_{\text{eq}}}, \quad (A7)$$

$$R \equiv 3\rho_b/4\rho_\gamma = 31.5\omega_b\Theta_{2.7}^{-4}(z/10^3)^{-1}, \quad (A8)$$

$$k_{\text{Silk}} = 1.6\omega_b^{0.52}\omega_0^{0.73} \left[1 + (10.4\omega_0)^{-0.95} \right] \text{Mpc}^{-1}, \quad (A9)$$

$$k_{\text{eq}} = 7.46 \times 10^{-2}\omega_0\Theta_{2.7}^{-2} \text{Mpc}^{-1}, \quad (A10)$$

$$\alpha_b = 2.07k_{\text{eq}}s(1 + R_d)^{-3/4}G \left(\frac{1 + z_{\text{eq}}}{1 + z_d} \right), \quad (A11)$$

$$\beta_b = 0.5 + \frac{\Omega_b}{\Omega_0} + \left(3 - 2\frac{\Omega_b}{\Omega_0} \right) \sqrt{(17.2\omega_0)^2 + 1}, \quad (A12)$$

$$s = \frac{2}{3k_{\text{eq}}} \sqrt{\frac{6}{R_{\text{eq}}}} \ln \frac{\sqrt{1 + R_d} + \sqrt{R_d + R_{\text{eq}}}}{1 + \sqrt{R_{\text{eq}}}}, \quad (A13)$$

$$\tilde{s} = s \left[1 + \left(\frac{\beta_{\text{node}}}{ks} \right)^3 \right]^{-1/3}, \quad (A14)$$

$$\beta_{\text{node}} = 8.41\omega_0^{0.435}, \quad (A15)$$

$$G(y) = -6y\sqrt{1+y} + y(2+3y)\ln\left(\frac{\sqrt{1+y}+1}{\sqrt{1+y}-1}\right), \quad (\text{A16})$$

$$y \equiv \frac{1+z_{\text{eq}}}{1+z}, \quad (\text{A17})$$

$$\alpha_c = a_1^{-\Omega_b/\Omega_0} a_2^{-(\Omega_b/\Omega_0)^3}, \quad (\text{A18})$$

$$a_1 = (46.9\omega_0)^{0.670}[1 + (32.1\omega_0)^{-0.532}], \quad (\text{A19})$$

$$a_2 = (12.0\omega_0)^{0.424}[1 + (45.0\omega_0)^{-0.582}], \quad (\text{A20})$$

$$\beta_c^{-1} = 1 + b_1[(\Omega_c/\Omega_0)^{b_2} - 1], \quad (\text{A21})$$

$$b_1 = 0.944[1 + (458\omega_0)^{-0.708}]^{-1}, \quad (\text{A22})$$

$$b_2 = (0.395\omega_0)^{-0.0266}. \quad (\text{A23})$$

$$z_{\text{eq}} = 2.50 \times 10^4 \omega_0 \Theta_{2.7}^{-4}, \quad (\text{A24})$$

$$z_d = 1291 \frac{\omega_0^{0.251}}{1 + 0.659\omega_0^{0.828}} \left[1 + b_{1,z} \omega_b^{b_{2,z}}\right], \quad (\text{A25})$$

$$b_{1,z} = 0.313\omega_0^{-0.419} [1 + 0.607\omega_0^{0.674}], \quad (\text{A26})$$

$$b_{2,z} = 0.238\omega_0^{0.223}, \quad (\text{A27})$$

where we have defined $\omega_0 = (\Omega_c + \Omega_b)h^2$, and $T_{\text{CMB}} \equiv 2.7\Theta_{2.7}\text{K}$, $R_d \equiv R(z_d)$ and $R_{\text{eq}} \equiv R(z_{\text{eq}})$.

- [1] S. L. Brunton, J. L. Proctor, and J. N. Kutz, “Discovering governing equations from data by sparse identification of nonlinear dynamical systems,” *Proceedings of the National Academy of Sciences* **113** no. 15, (2016) 3932–3937, [arXiv:1509.03580 \[math.DS\]](https://arxiv.org/abs/1509.03580).
- [2] D. Izzo, F. Biscani, and A. Mereta, “Differentiable Genetic Programming,” *arXiv e-prints* (2016) , [arXiv:1611.04766 \[cs.NE\]](https://arxiv.org/abs/1611.04766).
- [3] M. Schmidt and H. Lipson, “Distilling Free-Form Natural Laws from Experimental Data,” *Science* **324** (2009) 81–85.
- [4] M. Cranmer *et al.*, “Discovering Symbolic Models from Deep Learning with Inductive Biases,” [arXiv:2006.11287 \[cs.LG\]](https://arxiv.org/abs/2006.11287).
- [5] S.-M. Udrescu and M. Tegmark, “AI Feynman: a Physics-Inspired Method for Symbolic Regression,” *Sci. Adv.* **6** no. 16, (2020) eaay2631, [arXiv:1905.11481 \[physics.comp-ph\]](https://arxiv.org/abs/1905.11481).
- [6] S.-M. Udrescu, A. Tan, J. Feng, O. Neto, T. Wu, and M. Tegmark, “AI Feynman 2.0: Pareto-optimal symbolic regression exploiting graph modularity,” [arXiv:2006.10782 \[cs.LG\]](https://arxiv.org/abs/2006.10782).
- [7] Z. Liu and M. Tegmark, “Machine Learning Hidden Symmetries,” *Phys. Rev. Lett.* **128** no. 18, (2022) 180201, [arXiv:2109.09721 \[cs.LG\]](https://arxiv.org/abs/2109.09721).
- [8] J. R. Koza, *Genetic Programming: On the Programming of Computers by Means of Natural Selection*. The MIT Press, 1992.
- [9] SDSS Collaboration, M. Tegmark *et al.*, “The 3-D power spectrum of galaxies from the SDSS,” *Astrophys. J.* **606** (2004) 702–740, [arXiv:astro-ph/0310725](https://arxiv.org/abs/astro-ph/0310725).
- [10] BOSS Collaboration, S. Alam *et al.*, “The clustering of galaxies in the completed SDSS-III Baryon Oscillation Spectroscopic Survey: cosmological analysis of the DR12 galaxy sample,” *Mon. Not. Roy. Astron. Soc.* **470** no. 3, (2017) 2617–2652, [arXiv:1607.03155 \[astro-ph.CO\]](https://arxiv.org/abs/1607.03155).
- [11] S. Dodelson and F. Schmidt, *Modern Cosmology*. Elsevier Science, 2020.

- [12] L. Amendola *et al.*, “Cosmology and fundamental physics with the Euclid satellite,” *Living Rev. Rel.* **21** no. 1, (2018) 2, [arXiv:1606.00180 \[astro-ph.CO\]](https://arxiv.org/abs/1606.00180).
- [13] Euclid Collaboration, Y. Mellier *et al.*, “Euclid. I. Overview of the Euclid mission,” [arXiv:2405.13491 \[astro-ph.CO\]](https://arxiv.org/abs/2405.13491).
- [14] DESI Collaboration, A. G. Adame *et al.*, “DESI 2024 VI: Cosmological Constraints from the Measurements of Baryon Acoustic Oscillations,” [arXiv:2404.03002 \[astro-ph.CO\]](https://arxiv.org/abs/2404.03002).
- [15] Euclid Collaboration, A. Blanchard *et al.*, “Euclid preparation. VII. Forecast validation for Euclid cosmological probes,” *Astron. Astrophys.* **642** (2020) A191, [arXiv:1910.09273 \[astro-ph.CO\]](https://arxiv.org/abs/1910.09273).
- [16] J. B. Orjuela-Quintana, S. Nesseris, and W. Cardona, “Using machine learning to compress the matter transfer function T(k),” *Phys. Rev. D* **107** no. 8, (2023) 083520, [arXiv:2211.06393 \[astro-ph.CO\]](https://arxiv.org/abs/2211.06393).
- [17] J. B. Orjuela-Quintana, S. Nesseris, and D. Sapone, “Machine learning unveils the linear matter power spectrum of modified gravity,” *Phys. Rev. D* **109** no. 6, (2024) 063511, [arXiv:2307.03643 \[astro-ph.CO\]](https://arxiv.org/abs/2307.03643).
- [18] DESI Collaboration, A. G. Adame *et al.*, “DESI 2024 III: Baryon Acoustic Oscillations from Galaxies and Quasars,” [arXiv:2404.03000 \[astro-ph.CO\]](https://arxiv.org/abs/2404.03000).
- [19] D. J. Eisenstein and W. Hu, “Baryonic features in the matter transfer function,” *Astrophys. J.* **496** (1998) 605, [arXiv:astro-ph/9709112](https://arxiv.org/abs/astro-ph/9709112).
- [20] R. Poli, W. B. Langdon, and N. F. McPhee, *A Field Guide to Genetic Programming*. Lulu Enterprises, UK Ltd, 2008.
- [21] G. Carleo, I. Cirac, K. Cranmer, L. Daudet, M. Schuld, N. Tishby, L. Vogt-Maranto, and L. Zdeborová, “Machine learning and the physical sciences,” *Rev. Mod. Phys.* **91** no. 4, (2019) 045002, [arXiv:1903.10563 \[physics.comp-ph\]](https://arxiv.org/abs/1903.10563).
- [22] R. Lahoz-Beltra, “Solving the Schrödinger equation with genetic algorithms: a practical approach,” [arXiv:2210.15720 \[quant-ph\]](https://arxiv.org/abs/2210.15720).

[23] P. Berglund, Y.-H. He, E. Heyes, E. Hirst, V. Jejjala, and A. Lukas, “New Calabi–Yau manifolds from genetic algorithms,” *Phys. Lett. B* **850** (2024) 138504, [arXiv:2306.06159 \[hep-th\]](https://arxiv.org/abs/2306.06159).

[24] N. Gupte and I. Bartos, “Optimal Gravitational-wave Follow-up Tiling Strategies Using a Genetic Algorithm,” *Phys. Rev. D* **101** no. 12, (2020) 123008, [arXiv:2003.04839 \[astro-ph.IM\]](https://arxiv.org/abs/2003.04839).

[25] S. Q. Wu, M. C. Ji, Z. Wang, M. C. Nguyen, X. Zhao, K. Umemoto, R. M. Wentzcovitch, and K. M. Ho, “An adaptive genetic algorithm for crystal structure prediction,” *J. Phys.: Condens. Matter* **26** no. 3, (2013) 035402.

[26] X.-L. Luo, J. Feng, and H.-H. Zhang, “A genetic algorithm for astroparticle physics studies,” *Comput. Phys. Commun.* **250** (2020) 106818, [arXiv:1907.01090 \[astro-ph.HE\]](https://arxiv.org/abs/1907.01090).

[27] M. Ho *et al.*, “A Robust and Efficient Deep Learning Method for Dynamical Mass Measurements of Galaxy Clusters,” *Astrophys. J.* **887** (2019) 25, [arXiv:1902.05950 \[astro-ph.CO\]](https://arxiv.org/abs/1902.05950).

[28] R. Arjona and S. Nesseris, “What can Machine Learning tell us about the background expansion of the Universe?,” *Phys. Rev. D* **101** no. 12, (2020) 123525, [arXiv:1910.01529 \[astro-ph.CO\]](https://arxiv.org/abs/1910.01529).

[29] R. Arjona and S. Nesseris, “Hints of dark energy anisotropic stress using Machine Learning,” *JCAP* **11** (2020) 042, [arXiv:2001.11420 \[astro-ph.CO\]](https://arxiv.org/abs/2001.11420).

[30] G. Alestas, L. Kazantzidis, and S. Nesseris, “Machine learning constraints on deviations from general relativity from the large scale structure of the Universe,” [arXiv:2209.12799 \[astro-ph.CO\]](https://arxiv.org/abs/2209.12799).

[31] R. Medel-Esquivel, I. Gómez-Vargas, A. A. M. Sánchez, R. García-Salcedo, and J. Alberto Vázquez, “Cosmological Parameter Estimation with Genetic Algorithms,” *Universe* **10** no. 1, (2024) 11, [arXiv:2311.05699 \[astro-ph.CO\]](https://arxiv.org/abs/2311.05699).

[32] C. Bogdanos and S. Nesseris, “Genetic Algorithms and Supernovae Type Ia Analysis,” *JCAP* **05** (2009) 006, [arXiv:0903.2805 \[astro-ph.CO\]](https://arxiv.org/abs/0903.2805).

[33] S. Nesseris and A. Shafeloo, “A model independent null test on the cosmological constant,” *Mon. Not. Roy. Astron. Soc.* **408** (2010) 1879–1885, [arXiv:1004.0960 \[astro-ph.CO\]](https://arxiv.org/abs/1004.0960).

[34] R. Arjona and S. Nesseris, “Novel null tests for the spatial curvature and homogeneity of the Universe and their machine learning reconstructions,” *Phys. Rev. D* **103** no. 10, (2021) 103539, [arXiv:2103.06789 \[astro-ph.CO\]](https://arxiv.org/abs/2103.06789).

[35] R. Arjona, A. Melchiorri, and S. Nesseris, “Testing the Λ CDM paradigm with growth rate data and machine learning,” *JCAP* **05** no. 05, (2022) 047, [arXiv:2107.04343 \[astro-ph.CO\]](https://arxiv.org/abs/2107.04343).

[36] R. Arjona, H.-N. Lin, S. Nesseris, and L. Tang, “Machine learning forecasts of the cosmic distance duality relation with strongly lensed gravitational wave events,” *Phys. Rev. D* **103** no. 10, (2021) 103513, [arXiv:2011.02718 \[astro-ph.CO\]](https://arxiv.org/abs/2011.02718).

[37] **Euclid** Collaboration, M. Martinelli *et al.*, “Euclid: Forecast constraints on the cosmic distance duality relation with complementary external probes,” *Astron. Astrophys.* **644** (2020) A80, [arXiv:2007.16153 \[astro-ph.CO\]](https://arxiv.org/abs/2007.16153).

[38] **Euclid** Collaboration, S. Nesseris *et al.*, “Euclid: Forecast constraints on consistency tests of the Λ CDM model,” *Astron. Astrophys.* **660** (2022) A67, [arXiv:2110.11421 \[astro-ph.CO\]](https://arxiv.org/abs/2110.11421).

[39] J. K. Yadav, J. S. Bagla, and N. Khandai, “Fractal dimension as a measure of the scale of homogeneity,” *Month. Not. Roy. Astro. Soc.* **405** no. 3, (July, 2010) 2009–2015, [arXiv:1001.0617 \[astro-ph.CO\]](https://arxiv.org/abs/1001.0617).

[40] **Planck** Collaboration, N. Aghanim *et al.*, “Planck 2018 results. VI. Cosmological parameters,” *Astron. Astrophys.* **641** (2020) A6, [arXiv:1807.06209 \[astro-ph.CO\]](https://arxiv.org/abs/1807.06209). [Erratum: *Astron. Astrophys.* 652, C4 (2021)].

[41] S. Agarwal and H. A. Feldman, “The effect of massive neutrinos on the matter power spectrum,” *Month. Not. Roy. Astro. Soc.* **410** no. 3, (Jan., 2011) 1647–1654, [arXiv:1006.0689 \[astro-ph.CO\]](https://arxiv.org/abs/1006.0689).

[42] L. Lombriser, F. Simpson, and A. Mead, “Unscreening Modified Gravity in the Matter Power Spectrum,” *Phys. Rev. Lett.* **114** no. 25, (2015) 251101, [arXiv:1501.04961 \[astro-ph.CO\]](https://arxiv.org/abs/1501.04961).

[43] D. Blas, J. Lesgourgues, and T. Tram, “The Cosmic Linear Anisotropy Solving System (CLASS). Part II: Approximation schemes,” *Journal of Cosmology and Astroparticle Physics* **2011** no. 07, 034–034.

[44] A. Lewis, A. Challinor, and A. Lasenby, “Efficient computation of CMB anisotropies in closed FRW models,” *Astrophys. J.* **538** (2000) 473–476, [arXiv:astro-ph/9911177](https://arxiv.org/abs/astro-ph/9911177).

[45] G.-B. Zhao, L. Pogosian, A. Silvestri, and J. Zylberberg, “Searching for modified growth patterns with tomographic surveys,” *Phys. Rev. D* **79** (2009) 083513, [arXiv:0809.3791 \[astro-ph\]](https://arxiv.org/abs/0809.3791).

[46] A. Zucca, L. Pogosian, A. Silvestri, and G.-B. Zhao, “MGCAMB with massive neutrinos and dynamical dark energy,” *JCAP* **05** (2019) 001, [arXiv:1901.05956 \[astro-ph.CO\]](https://arxiv.org/abs/1901.05956).

[47] Z. Wang, S. H. Mirpoorian, L. Pogosian, A. Silvestri, and G.-B. Zhao, “New MGCAMB tests of gravity with CosmoMC and Cobaya,” *JCAP* **08** (2023) 038, [arXiv:2305.05667 \[astro-ph.CO\]](https://arxiv.org/abs/2305.05667).

[48] M. Zumalacárregui, E. Bellini, I. Sawicki, J. Lesgourgues, and P. G. Ferreira, “hi_class: Horndeski in the Cosmic Linear Anisotropy Solving System,” *JCAP* **08** (2017) 019, [arXiv:1605.06102 \[astro-ph.CO\]](https://arxiv.org/abs/1605.06102).

[49] Z. Saki and M. Martinelli, “Cosmological constraints on sub-horizon scales modified gravity theories with MGCLASS II,” *JCAP* **05** no. 05, (2022) 030, [arXiv:2112.14175 \[astro-ph.CO\]](https://arxiv.org/abs/2112.14175).

[50] N. Becker, D. C. Hooper, F. Kahlhoefer, J. Lesgourgues, and N. Schöneberg, “Cosmological constraints on multi-interacting dark matter,” *JCAP* **02** (2021) 019, [arXiv:2010.04074 \[astro-ph.CO\]](https://arxiv.org/abs/2010.04074).

[51] F. Villaescusa-Navarro *et al.*, “The Quijote simulations,” *Astrophys. J. Suppl.* **250** no. 1, (2020) 2, [arXiv:1909.05273 \[astro-ph.CO\]](https://arxiv.org/abs/1909.05273).

[52] K. Heitmann, E. Lawrence, J. Kwan, S. Habib, and D. Higdon, “The Coyote Universe Extended: Precision Emulation of the Matter Power Spectrum,” *Astrophys. J.* **780** (2014) 111, [arXiv:1304.7849 \[astro-ph.CO\]](https://arxiv.org/abs/1304.7849).

[53] R. E. Angulo, M. Zennaro, S. Contreras, G. Aricò, M. Pellejero-Ibañez, and J. Stüber, “The BACCO simulation project: exploiting the full power of large-scale structure for cosmology,” *Mon. Not. Roy. Astron. Soc.* **507** no. 4, (2021) 5869–5881, [arXiv:2004.06245 \[astro-ph.CO\]](https://arxiv.org/abs/2004.06245).

[54] A. Mootoovaloo, A. H. Jaffe, A. F. Heavens, and F. Leclercq, “Kernel-based emulator for the 3D matter power spectrum from CLASS,” *Astron. Comput.* **38** (2022) 100508, [arXiv:2105.02256 \[astro-ph.CO\]](https://arxiv.org/abs/2105.02256).

[55] A. Spurio Mancini, D. Piras, J. Alsing, B. Joachimi, and M. P. Hobson, “CosmoPower: emulating cosmological power spectra for accelerated Bayesian inference from next-generation surveys,” *Mon. Not. Roy. Astron. Soc.* **511** no. 2, (2022) 1771–1788, [arXiv:2106.03846 \[astro-ph.CO\]](https://arxiv.org/abs/2106.03846).

[56] D. J. Bartlett, L. Kammerer, G. Kronberger, H. Desmond, P. G. Ferreira, B. D. Wandelt, B. Burlacu, D. Alonso, and M. Zennaro, “A precise symbolic emulator of the linear matter power spectrum,” *Astron. Astrophys.* **686** (2024) A209, [arXiv:2311.15865 \[astro-ph.CO\]](https://arxiv.org/abs/2311.15865).

[57] D. J. Bartlett, B. D. Wandelt, M. Zennaro, P. G. Ferreira, and H. Desmond, “syren-halofit: A fast, interpretable, high-precision formula for the Λ CDM nonlinear matter power spectrum,” *Astron. Astrophys.* **686** (2024) A150, [arXiv:2402.17492 \[astro-ph.CO\]](https://arxiv.org/abs/2402.17492).

[58] J. M. Bardeen, J. R. Bond, N. Kaiser, and A. S. Szalay, “The Statistics of Peaks of Gaussian Random Fields,” *Astroph. Jour.* **304** (May, 1986) 15.

[59] H. Winther, S. Casas, M. Baldi, K. Koyama, B. Li, L. Lombriser, and G.-B. Zhao, “Emulators for the nonlinear matter power spectrum beyond Λ CDM,” *Phys. Rev. D* **100** no. 12, (2019) 123540, [arXiv:1903.08798 \[astro-ph.CO\]](https://arxiv.org/abs/1903.08798).

[60] **LSST Dark Energy Science** Collaboration, N. Ramachandra, G. Valogiannis, M. Ishak, and K. Heitmann, “Matter Power Spectrum Emulator for f(R) Modified Gravity Cosmologies,” *Phys. Rev. D* **103** no. 12, (2021) 123525, [arXiv:2010.00596 \[astro-ph.CO\]](https://arxiv.org/abs/2010.00596).

[61] B. Fiorini, K. Koyama, and T. Baker, “Fast production of cosmological emulators in modified gravity: the matter power spectrum,” *JCAP* **12** (2023) 045, [arXiv:2310.05786 \[astro-ph.CO\]](https://arxiv.org/abs/2310.05786).

[62] S. R. Hinton *et al.*, “Measuring the 2D Baryon Acoustic Oscillation signal of galaxies in WiggleZ: Cosmological constraints,” *Mon. Not. Roy. Astron. Soc.* **464** no. 4, (2017) 4807–4822, [arXiv:1611.08040 \[astro-ph.CO\]](https://arxiv.org/abs/1611.08040).

[63] **Euclid** Collaboration, S. Casas *et al.*, “Euclid: Constraints on f(R) cosmologies from the spectroscopic and photometric primary probes,” [arXiv:2306.11053 \[astro-ph.CO\]](https://arxiv.org/abs/2306.11053).

[64] S.-F. Chen *et al.*, “Baryon Acoustic Oscillation Theory and Modelling Systematics for the DESI 2024 results,” [arXiv:2402.14070 \[astro-ph.CO\]](https://arxiv.org/abs/2402.14070).

[65] A. Aizpuru, R. Arjona, and S. Nesseris, “Machine learning improved fits of the sound horizon at the baryon drag epoch,” *Phys. Rev. D* **104** no. 4, (2021) 043521, [arXiv:2106.00428 \[astro-ph.CO\]](https://arxiv.org/abs/2106.00428).

[66] **BOSS** Collaboration, A. J. Ross *et al.*, “The clustering of galaxies in the completed SDSS-III Baryon Oscillation Spectroscopic Survey: Observational systematics and baryon acoustic oscillations in the correlation function,” *Mon. Not. Roy. Astron. Soc.* **464** no. 1, (2017) 1168–1191, [arXiv:1607.03145 \[astro-ph.CO\]](https://arxiv.org/abs/1607.03145).

[67] **eBOSS** Collaboration, J. E. Bautista *et al.*, “The Completed SDSS-IV extended Baryon Oscillation Spectroscopic Survey: measurement of the BAO and growth rate of structure of the luminous red galaxy sample from the anisotropic correlation function between redshifts 0.6 and 1,” *Mon. Not. Roy. Astron. Soc.* **500** no. 1, (2020) 736–762, [arXiv:2007.08993 \[astro-ph.CO\]](https://arxiv.org/abs/2007.08993).

[68] D. J. Eisenstein and W. Hu, “Power spectra for cold dark matter and its variants,” *Astrophys. J.* **511** (1997) 5, [arXiv:astro-ph/9710252](https://arxiv.org/abs/astro-ph/9710252).

[69] **Planck** Collaboration, P. A. R. Ade *et al.*, “Planck 2015 results. XIV. Dark energy and modified gravity,” *Astron. Astrophys.* **594** (2016) A14, [arXiv:1502.01590 \[astro-ph.CO\]](https://arxiv.org/abs/1502.01590).

[70] **DES** Collaboration, T. M. C. Abbott *et al.*, “Dark Energy Survey Year 1 Results: Constraints on Extended Cosmological Models from Galaxy Clustering and Weak Lensing,” *Phys. Rev. D* **99** no. 12, (2019) 123505, [arXiv:1810.02499 \[astro-ph.CO\]](https://arxiv.org/abs/1810.02499).